Translational Stroke Research (2021) 12:1035–1044
https://doi.org/10.1007/s12975-021-00893-6

ORIGINAL ARTICLE

Clinical Value of 3D-Printed Navigation Technology Combined with Neuroendoscopy for Intracerebral Hemorrhage

Yuqian Li[1] · Hongyu Cheng[2] · Zhenzhu Li[3] · Haikang Zhao[4] · Jiancai Wang[5] · Peng Wang[6] · Tongxin Jin[7] · Guiyong Zheng[8] · Haoxiang Ye[9] · Shaopeng Li[10] · Jun Zhang[6]

Received: 29 October 2020 / Revised: 3 January 2021 / Accepted: 17 January 2021 / Published online: 25 January 2021

Abstract

Intracerebral hemorrhage (ICH) is the most common form of hemorrhagic stroke with high morbidity and mortality. Rapid and massive bleeding may compress the brain tissue, causing space-occupying and pathological effects, such as reduced local cerebral blood flow, acidosis, and inflammatory and immune responses. Although the development of minimally invasive technique provides a new option for the treatment of ICH, their application is limited due to the difficulty in achieving accurate puncture localization under the guidance of the marks on CT. We selected 30 patients treated with neuroendoscopic surgery guided by 3D-printed navigation technology (experimental group) and 30 patients treated with neuroendoscopic surgery guided by hand-painted on the patient's body surface according to the marks on CT (control group). Our results showed that patients in the experimental group had a lower number of intraoperative punctures, shorter operation time, less intraoperative blood loss, higher hematoma clearance rate, and smaller volume of perihematomal edema than the patients in the control group. Moreover, patients in the experimental group had higher Glasgow Coma Scale score at discharge, shorter postoperative hospitalization time and ICU stay, and a lower rate of postoperative complications, despite the lack of statistically significant differences. In addition, no statistically significant differences were observed in mortality and Glasgow Outcome Scale score between the two groups. In conclusion, 3D-printed navigation technology used for the neuroendoscopic hematoma removal is a more reliable and less invasive approach in the treatment of ICH. This technique has great application prospects and deserves promotion in the future clinical practice.

Keywords Intracerebral hemorrhage · 3D-printed navigation technology · Neuroendoscopic surgery · Clearance of hematoma

Yuqian Li, Hongyu Cheng, and Zhenzhu Li contributed equally to this study.

✉ Shaopeng Li
shaopengli333@126.com

✉ Jun Zhang
24451526@qq.com

[1] Department of Neurosurgery, Tangdu Hospital, Air Force Medical University, Xi'an, Shaanxi, China

[2] Department of Ultrasound Diagnosis, Tangdu Hospital, Air Force Medical University, Xi'an, Shaanxi, China

[3] Department of Neurosurgery, Binzhou Medical University Hospital, Binzhou, Shandong, China

[4] Department of Neurosurgery, The Second Hospital Affiliated of Xi'an Medical University, Xi'an, Shaanxi, China

[5] Department of Neurosurgery, PLA 982 hospital, Tangshan, Hebei, China

[6] Department of Neurosurgery, Dalang Hospital, Dongguan, Guangdong, China

[7] Department of Intensive Care Unit, Dalang Hospital, Dongguan, Guangdong, China

[8] Department of Anesthesiology, Dalang Hospital, Dongguan, Guangdong, China

[9] Department of Radiology, Dalang Hospital, Dongguan, Guangdong, China

[10] Department of Neurosurgery, Dongguan People's Hospital, Affiliated Dongguan People's Hospital of Southern Medical University, Dongguan, China

Introduction

Intracerebral hemorrhage (ICH) is a common neurological emergency characterized by rapid onset and high mortality and disability, accounting for approximately 10–30% of all strokes [1–3]. Currently, conservative treatment and surgical intervention of hematoma clearance are the main treatment of ICH [4]. Surgical hematoma clearance cannot only quickly remove the hematoma and reduce intracranial pressure, but decrease the secondary brain damage caused by erythrocyte lysis or other neurotoxic chemicals and thus protecting the survival tissues [5–7]. At present, the most commonly used methods of hematoma removal are craniotomy, minimally invasive drainage, and neuroendoscopy [8–10]. Neuroendoscopic intracranial hematoma clearance combines the advantages of craniotomy and minimal puncture drainage and can remove most of the hematoma directly and less invasively achieving a higher degree of satisfaction and a better postoperative prognosis operation [11]. However, the biggest problem to its application in clinical practice is the difficulty to accurately locate the position based on the hand-painted localization under the guidance of the marks on preoperative CT. The puncture deviation during operation may lead to serious risks and consequences, such as damage to the surrounding brain tissue and vital blood vessels or nerves, and the result of the surgery may be unsatisfactory [12]. Therefore, finding a new method to improve the puncture accuracy and reduce the occurrence of puncture deviation is an important direction to improve the outcomes of neuroendoscopic intracranial hematoma clearance.

Three-dimensional (3D)-printed technology is a rapid prototyping technology based on the use of digital model files [13]. It can print a solid object form with complex geometry through multilayer processing [14, 15]. Three-dimensionally printed technology has been increasingly widely applied in clinical medicine along with its advancing maturity [16, 17]. In the present study, we used 3D-printed technology to construct an individualized navigation model to achieve a precise puncture during neuroendoscopic intracranial hematoma clearance. The position and shape of the hematoma are analyzed under the guidance of the digital imaging and communications in medicine (DICOM) data of the patient's head CT. Then, the puncture route containing the puncture entry point, direction, angle, and depth is determined, and the individualized navigation model is developed using 3D printing technology. The 3D-printed navigation technology can reduce the tissue damage because of the deviation caused by the instrument swing or positioning during the puncture process, and improve the accuracy of neuroendoscopic intracranial hematoma clearance.

Materials and Methods

Patients and Tissue Samples

From January 2017 to January 2020, 60 patients (30 males and 30 females, aged 38–83 years) with ICH who were admitted to the Department of Neurosurgery of Tangdu Hospital (Air Force Medical University, Xi'an, China) and Dalang Hospital (Dongguan, Guangdong, China) with complete medical records were selected. All the patients had signed the informed consent before surgery; the coma patients were signed by their immediate family members. Patients were selected according to the following criteria: (1) spontaneous ICH in the basal ganglia; (2) hematoma volume > 30 mL; (3) Glasgow Coma Scale (GCS) > 4, no cerebral hernia and stable vital signs; (4) age > 18 years. The following exclusion criteria were applied: (1) ICH caused by intracranial aneurysms, cerebral arteriovenous malformations, and other brain diseases; (2) any previous history of serious heart, liver, kidney, or other substantial organ dysfunction diseases; (3) coagulation dysfunction; (4) patients with AIDS or other immunodeficiency diseases; (5) lost follow-up. Thirty patients with ICH that were treated with neuroendoscopic surgery guided by 3D-printed navigation technology were categorized as the experimental group ($n = 30$). The other 30 patients were treated by neuroendoscopic surgery guided by hand-painted localization on the patient's body surface according to the CT marks composed the control group ($n = 30$). Patients were followed up for 6 months from the date of surgery. The basic preoperative data of the patients in the two groups are listed in Table 1.

Surgical Methods

Experimental Group

The patients underwent thin-slice computed tomography (CT) scanning to obtain the DICOM data. These data was entered into the computer and Mimics16.0 software was run. Then, the 3D reconstruction model consisting of the morphology, location, size and depth of the hematoma in the brain was developed. Based on the 3D reconstruction model, we designed the optimal puncture path which was directed to the hematoma center avoiding important structures, which contained the puncture entry point and the direction, angle, and depth of the intervention. The corresponding individualized 3D-printed model with extracranial navigation guide plate was further printed using a 3D printer (CASET 250MC, China). After printing, the 3D-printed facial model was placed on the head of the patient to ensure that the model was closely approximated to the patient's face to avoid puncture deviation caused by poor fit (Fig. 1).

Table 1 Clinical baseline parameters

Clinical parameters	Experimental group (30)	Control group (30)	*P*
Female (*n*/%)	16/53.3	14/46.7	0.606
Age (years)	62.5 ± 10.4	59.2 ± 10.2	0.212
HV (mL)	55.1 ± 11.9	56.4 ± 13.4	0.693
30–60 mL	23/76.7	24/80.0	0.754
> 60 mL	7/23.3	6/20.0	
Location			
Left	18/60.0	14/46.7	0.301
Right	12/40.0	16/53.3	
GCS (score)	7.8 ± 1.8	8.0 ± 1.9	0.837
4–8	18/60.0	16/53.3	0.602
9–14	12/40.0	14/46.7	
Weight (kg)	68.8 ± 12.9	65.7 ± 13.6	0.360
SBP (mmHg)	166.3 ± 11.7	169.0 ± 11.5	0.365
Printing time of model	1.49 ± 0.13	0	0.000
Time from admission to surgery (h)	4.7 ± 1.0	4.4 ± 0.9	0.301
Platelets ($\times 10^9$ cells/L)	207.5 ± 41.3	212.2 ± 37.5	0.644
INR	1.0036 ± 0.091	1.0060 ± 0.095	0.925
Creatinine (umol/L)	64.8 ± 16.7	67.4 ± 15.6	0.537
IVH (*n*/%)	2/6.7	4/13.3	0.671
History of hypertension (*n*/%)	26/86.7	27/90.0	0.688
Diabetes (*n*/%)	7/23.3	5/16.7	0.519

HV, hematoma volume; *GCS*, Glasgow Coma Scale; *SBP*, systolic blood pressure; *INR*, international normalized ratio; *IVH*, intraventricular hemorrhage

Neuroendoscopic Hematoma Removal

General anesthesia was performed, and the surgical area was locally disinfected. The personalized 3D-printed navigation model was wrapped with a sterile film and was closely approximated to the patient's face. Then, the puncture site and surgical incision location were determined according to the puncture hole determined by the model. A 5–6-cm incision was made at the puncture site, and the skin, subcutaneous tissue, and aponeurosis layer were successively cut to reveal the surgical field. Next, the approximately 3-cm-diameter bone flap was removed with a milling cutter, and the dura mater was cut longitudinally. Under the guidance of the navigation model, the disposable tissue guide expander was punctured into the hematoma cavity based on the preoperative design. Then, the obturator was removed and a syringe was used to suck the hematoma to reduce the pressure. After the successful puncture of the hematoma was confirmed, the transparent working sheath was inserted, and the puncture device was removed. Furthermore, the neuroendoscope was inserted into the transparent working sheath to observe the boundary between the hematoma and the brain tissue. Under neuroendoscopy monitoring, an aspirator rotating in a certain direction was used to gradually remove the surrounding hematoma. Then, the suction device with the function of single-electrode electrocoagulation was used to solidify the bleeding point, so as to reliably stop the bleeding. After carefully inspecting and confirming the absence of obvious blood clots and active bleeding around the working sheath, the hematoma cavity was rinsed and the guide and transparent working sheath were removed. Next, we observed whether a significant gap between the inner skull plate and brain tissue was present to judge whether adequate stress reduction was achieved. A drainage tube was placed in the hematoma cavity, the dura mater was repaired, and the bone flap was restored. The retained periosteum flap was used to cover the bone flap to prevent postoperative cerebrospinal fluid leakage. Finally, the scalp cortex was sutured successively (Fig. 2).

Control Group

We determined the puncture entry point and the direction, angle, and depth by hand-painted localization on the patient's body surface according to the marks of the preoperative CT scan measurements. Under general anesthesia, local disinfection was carried out in the operating area, and routine towels were laid. The craniotomy process was the same as that of the experimental group. Under the visual inspection of a surgeon and an assistant, the disposable tissue guide dilator was used to create a puncture to the hematoma cavity. Furthermore, the

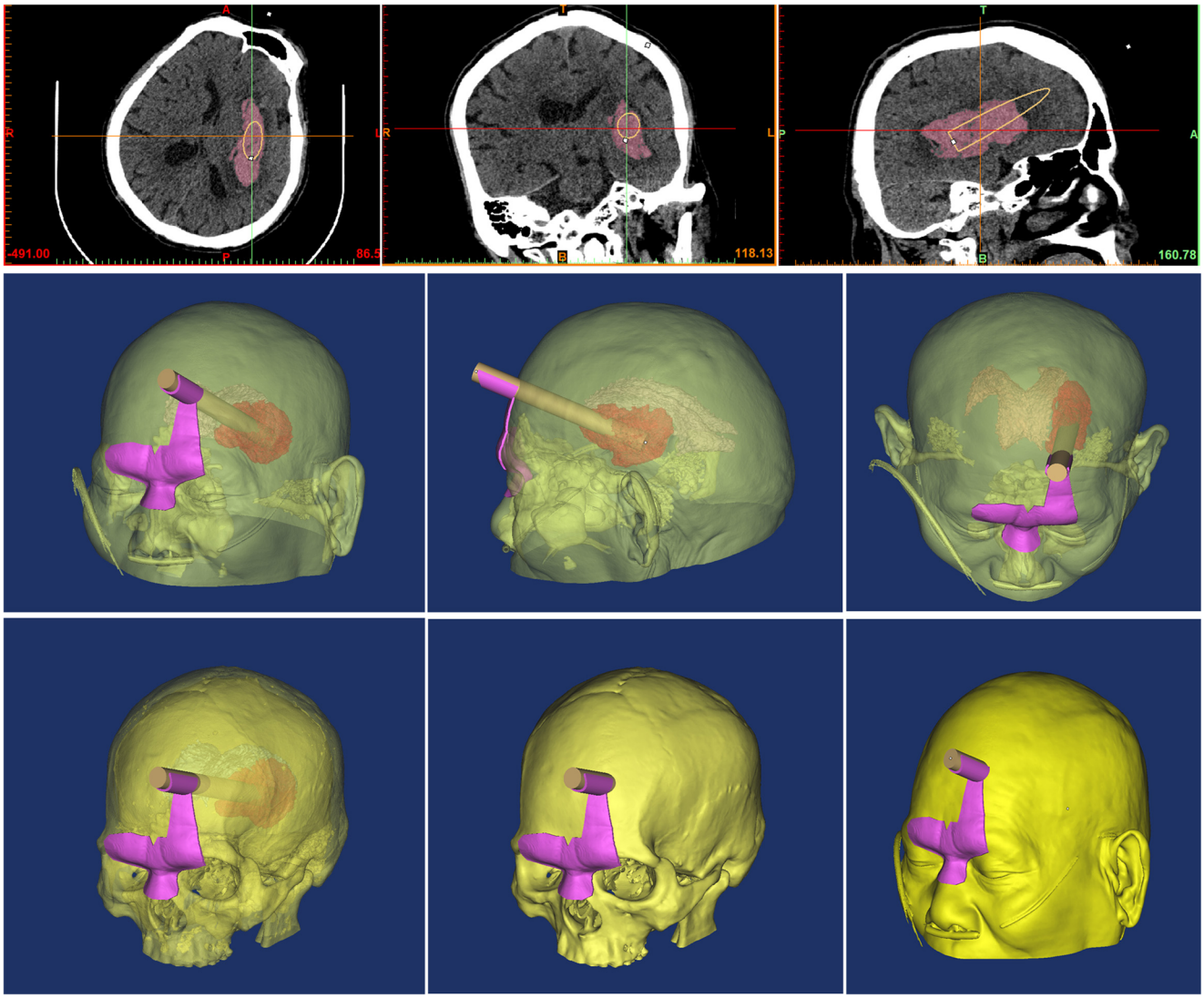

Fig. 1 Preoperative computer-assisted optimal design of the puncture passage and 3D reconstruction were used to determine the trajectory of the puncturing needle

occluder was removed, and the hematoma was sucked with a syringe to reduce the pressure. After the successful puncture of hematoma was confirmed, the transparent working sheath was placed and the puncture device was replaced by a neuroendoscope. Then, by adjusting the angle of the transparent working sheath, we detected and removed the hematoma as much as possible.

Postoperative Evaluation

The patients in both groups underwent routine postoperative CT examinations. We closely monitored the patients' vital signs and ensured that the body temperature and the electrolyte and blood glucose levels were maintained within the normal range; we strictly controlled their postoperative blood pressure and actively prevented complications. We also compared and analyzed the operation time, intraoperative blood loss, hematoma clearance rate, rebleeding, in-ICU stay, total hospital stay, Glasgow Coma Scale (GCS) score at discharge and complications of the two groups. The postoperative hospital mortality and Glasgow Outcome Scale (GOS) score was used as a prognostic index of patients 6 months postoperatively.

Statistical Methods

SPSS 16.0 (SPSS Inc., Chicago, IL, USA) was used to analyze and process the data of the patients in both groups. Continuous variables were verified for normality using the Kolmogorov–Smirnov test. The comparison of normally distributed variables was carried out by independent sample t test, and the results are represented as ($\bar{x} \pm s$). Categorical variables were compared using the chi-square test. $P < 0.05$ indicates statistically significant differences.

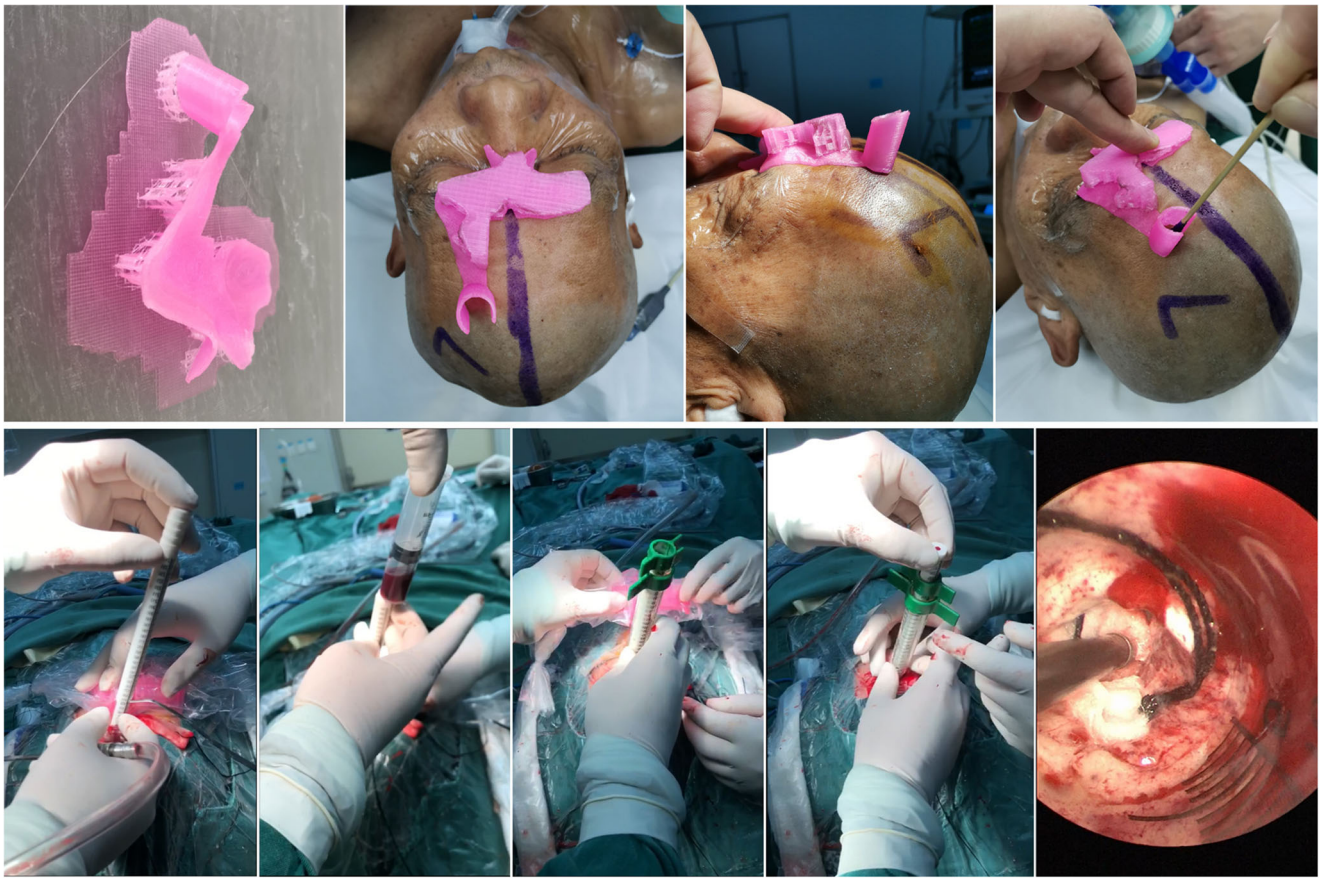

Fig. 2 The personalized 3D-printed navigation model was constructed and the navigation model was closely approximated to the patient's face. Under the guidance of the navigation model, the disposable tissue guide expander was punctured into the hematoma cavity based on the preoperative design

Results

Baseline Characteristics

A total number of 60 patients with ICH were enrolled in the study and were divided into two groups: 30 patients treated with neuroendoscopic surgery guided by 3D-printed guidance plate technology were allocated to the experimental group and 30 patients treated with neuroendoscopic surgery guided by hand-painted on the patient's body surface according to the marks of CT were included to the control group. The preoperative data of the two groups were collected and sorted out (summarized in Table 1); the demographic and clinical features did not significantly differ between the two groups.

Surgery-Associated Variables

The relevant surgery-associated variables are presented in Table 2. The operation time in the experimental group (104.3 ± 14.0 min) was significantly lower than that in the control group (118.6 ± 15.1 min, $P < 0.001$). Correspondingly, a smaller volume of intraoperative blood loss was observed in the experimental group (40.9 ± 13.4 mL versus 50.9 ± 15.7 mL in the control group, $P = 0.011$). The number of intraoperative punctures in the experimental group was only one, whereas in the control group, seven cases underwent the procedure twice (23.3%) and one three times (3.3%, $P = 0.01$). One (3.33%) of the patients in the control group received blood transfusions (i.e., red blood cell and blood plasma transfusions) during the operation versus no patients in the experimental group receiving transfusions ($P = 1.000$). No significant difference was observed between the two groups in the drain placement in the hematoma cavity during the surgery ($P = 0.301$).

Postoperative outcomes

The postoperative clinical characteristics of patients are displayed in Table 3. The evacuation rate on postoperative day 1 in the experimental group (93.5 ± 5.0%) was significantly higher than that in the control group (90.3 ± 5.9%, $P = 0.024$). On postoperative day 3, no significant differences were found between the two groups in the evacuation rate (97.5 ± 2.3% versus 96.3 ± 2.9%, $P = 0.092$).

Table 2 Variables associated with surgery

Variable	Experimental group (30)	Control group (30)	*P*
Operation time (min)	104.3 ± 14.0	118.6 ± 15.1***	< 0.001
Blood loss (mL)	40.9 ± 13.4	50.9 ± 15.7*	0.011
Blood transfusion (*n*/%)	0/0	1/3.3	1.000
Drain placement in hematoma cavity (*n*/%)	14/46.7	18/60.0	0.301
Number of intraoperative puncture (*n*/%)			
1	30/100	22/73.4	0.010
2	0/0	7/23.3	
3	0/0	1/3.3	

*$P < 0.05$; ***$P < 0.001$

Perihematomal edema (PHE) was examined on day 7 after the operation, and it was smaller in the experimental group (64.3 ± 12.2 mL) than in the control group (71.3 ± 13.5 mL, $P = 0.040$). In addition, the GCS in the experimental group on postoperative days 1, 3, and 7 was slightly higher than that in the control group, but the differences were not statistically significant ($P = 0.552$, 0.216, and 0.474, respectively). Moreover, statistical analyses revealed no significant association between the two groups concerning the number of patients treated with urokinase and the catheter-retained time ($P = 0.671$ and 0.194, respectively) (Fig. 3).

Postoperative Complications

No significant difference in the surgery-related complications between the two groups was observed (Table 4). None of the patients suffered from rebleeding in the experimental group, whereas one patient in the control group had that complication (0% versus 3.3%, $P = 0.313$). Moreover, statistical analyses revealed no significant differences between the two groups in the occurrence of postoperative complications, including infectious meningitis, pulmonary infection, digestive tract ulcer, and epilepsy ($P = 0.554$, 0.519, 0.488, and 0.706, respectively). Additionally, no patient in the experimental and control groups suffered from cerebral infarction and underwent reoperation.

Outcomes at Discharge and Long-Term Prognosis

The data of the surgical details, the clinical outcomes at discharge, and the long-term prognosis 6 months after the surgery are listed in Table 5. There was no significant difference in the GCS at discharge, total expenses, in-ICU stay, and in-hospital stay between the two groups ($P = 0.495$, 0.803, 0.208, and 0.831, respectively). After 6 months of follow-up, the mortality rates in the experimental group and control group were 6.7% (2/30) and 10.0% (3/30), respectively ($P = 0.640$). Additionally, none of the patients in the two groups was readmitted during the 3-month period after the discharge. The GOS score data were collected of all surviving patients, and further statistical analyses showed no difference in the GOS score between the two groups ($P = 0.702$).

Discussion

ICH is the most common type of hemorrhagic stroke and a neurological emergency causing high mortality and disability [18, 19]. Currently, two main treatment approaches are applied: non-surgical and surgical treatment. Non-surgical treatment, which is also called conservative treatment, includes monitoring the vital signs and state of consciousness at any time, dehydration to reduce intracranial pressure, nutritional

Table 3 Postoperative outcomes

Clinical outcomes	Experimental group (30)	Control group (30)	*P*
ER on day 1 (%)	93.5 ± 5.0	90.3 ± 5.9*	0.024
GCS on day 1 (score)	9.3 ± 1.6	9.1 ± 1.9	0.552
ER on day 3 (%)	97.5 ± 2.3	96.3 ± 2.9	0.092
GCS on day 3 (score)	11.0 ± 2.0	10.3 ± 2.3	0.216
PHE on day 7 (mL)	64.3 ± 12.2	71.3 ± 13.5*	0.040
GCS on day 7 (score)	12.0 ± 2.5	11.5 ± 2.9	0.474
Application of urokinase (*n*/%)	2/6.7	4/13.3	0.671
Catheter-retained time (day)	1.47 ± 0.57	1.67 ± 0.61	0.194

ER, evacuation rate; *GCS*, Glasgow Coma Scale; *PHE*, perihematomal edema

*$P < 0.05$

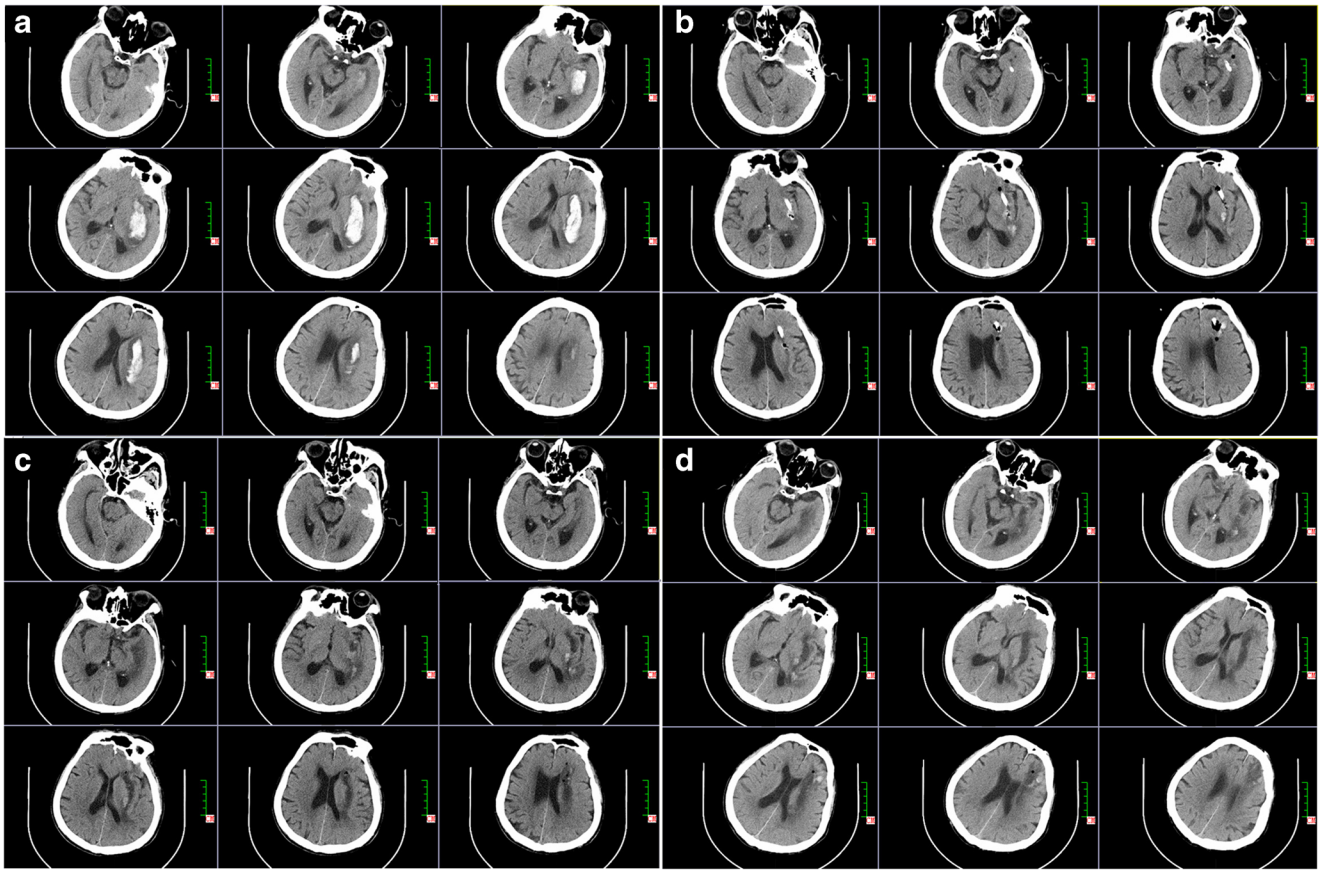

Fig. 3 A patient with ICH in left basal ganglia region received 3D-printed model-guided endoscopic evacuation. **a** Noncontrast computed tomography (CT) before operation. **b** Noncontrast CT on postoperative day 1. **c** Noncontrast CT on postoperative day 3. d Noncontrast CT on postoperative day 7

nerve treatment, prevention of complications, and nutritional support [20]. Surgical treatment is widely implemented in patients with larger hematoma volumes. A beneficial effect of surgery is the reduction of the physical forces of intracerebral hematoma. Surgery is used to directly remove the intracranial hematoma, decrease the intracranial pressure, and relieve the pressure of the hematoma on the brain and the nerve vessels. Beyond reducing the space-occupying effect, the removal of blood may also diminish the toxic stimulation and inflammatory cascades of the decomposition of the hematoma occurring in the brain tissue, thereby attenuating secondary brain damage [21]. Craniotomy, a traditional surgical approach, has the advantages of removing the intracranial hematoma with a high clearance rate and a rapid reduction of the intracranial pressure. However, a longer operation time is needed; larger intraoperative bleeding and bigger wounds to the surrounding brain are caused during operation [22]. In addition, serious complications may occur, such as surgical dysfunction, difficult incision healing, cerebrospinal fluid seepage, and postoperative intracranial infection. Moreover, some patients need to undergo cranial repair after a few months, which places not only considerable physiological,

Table 4 Postoperative complications

Clinical outcomes	Experimental group (30)	Control group (30)	*P*
Rebleeding (*n*/%)	0/0	1/3.3	0.313
Infectious meningitis (*n*/%)	1/3.3	2/6.7	0.554
Pulmonary infection (*n*/%)	5/16.7	7/23.3	0.519
Digestive tract ulcer (*n*/%)	4/13.3	6/20.0	0.488
Epilepsy (*n*/%)	3/10	5/16.7	0.706
Cerebral infarction (*n*/%)	0/0	0/0	-
Reoperation (*n*/%)	0/0	0/0	-

Table 5 Outcomes at discharge and long-term prognosis

Clinical outcomes	Experimental group (30)	Control group (30)	*P*
GCS at discharge (score)	12.4 ± 2.7	11.9 ± 3.3	0.495
Total expenses (ten thousand yuan)	7.5 ± 1.4	7.4 ± 1.6	0.803
In-ICU stay (day)	3.0 ± 1.2	3.4 ± 1.3	0.208
In-hospital stay (day)	8.8 ± 3.1	9.0 ± 2.9	0.831
Re-admission within 3 months after discharge (*n*/%)	0/0	0/0	-
Case fatality (*n*/%)	2/6.7	3/10.0	0.640
GOS (score)	3.6 ± 1.1	3.5 ± 0.9	0.702

GCS, Glasgow Coma Scale; *GOS*, Glasgow Outcome Scale; *ICU*, intensive care unit

but also heavy psychological and economic burden on patients.

Currently, the application of less invasive surgical approaches for ICH treatment has been increasingly extended. The advantages of recently developed methods for minimally invasive puncture and neuroendoscopy, such as reduced trauma, fewer complications, and quick recovery after operation, have been gradually recognized [23]. It is noteworthy that although minimally invasive drainage can prevent considerable tissue and bone flap damage, there are still some shortcomings to be overcome, including postoperative residual hematoma that needs further drug-assisted excretion; bleeding point hemostasis is difficult to effectively achieve during the operation, and probability of rebleeding and infection is higher [24]. Importantly, neuroendoscopic intracranial hematoma clearance is now considered a safe and effective surgical procedure, which combines the advantages of craniotomy and minimally invasive drainage. It cannot only accurately remove hematoma under the endoscopic direct vision, but also detect the bleeding point and rapidly perform electrocoagulation hemostasis [25]. Under neuroendoscopy guidance, damage of the important blood vessels and nerves in the brain tissue can be avoided. Besides, it has the advantages of complete clearance of hematoma, more reliable hemostasis, and high postoperative patient satisfaction [26]. However, at present, surface positioning by hand-painted localization under the guidance of the marks on CT is still used to perform neuroendoscopy, and thus, the accuracy of puncture positioning is poor. An angle deviation or a swing of the instrument may occur during the puncture process, which may cause serious damage to the surrounding normal brain tissue. Hence, finding new methods to improve the puncture accuracy has attracted significant research attention in recent years [27].

Nowadays, the increasing use of 3D printing technology in the medical field enables the achievement of the goal of improving puncture accuracy [28]. Based on imaging data, we reconstructed the individualized cephalic and facial models of the patients. This allowed the design of the optimal puncture passage. The precise puncture position, angle, and depth were set according to the location and shape of the hematoma. Then, the individualized 3D-printed navigation model was printed out by a 3D printer. During the operation, the 3D-printed navigation model was firmly adhered to the maxillofacial region. With its help, the transparent working sheath was accurately inserted into the hematoma center, preventing any puncture deviation and potentially repeated puncture caused by subjective, operator-related factors, and thereby avoiding the damage of important brain tissues. The operation process is smoother and more accurate, which not only shortens the operation time but eliminates the need for repeated puncture and minimizes the possibility of an instrument swing during the operation, thus reducing the injury caused to the normal brain tissue along the puncture path.

In the present study, we attempted to validate the clinical value of 3D-printed technology combined with neuroendoscopy for the treatment of ICH. To the best of our knowledge, no study has compared the difference between an operation with and without neuroendoscopic surgery guided by 3D-printed navigation technology. We first used 3D printing software Mimics 16.0 for 3D reconstruction according to the data of the preoperative thin-slice CT data. Then, we rapidly designed the personalized face 3D-printed navigation model with a puncture hole and a fixed puncture angle before the operation. The design of the navigation model using Mimics16.0 software took only 10–20 min. Afterwards, the model was printed by a 3D printer, which required another 1.5 h. Theoretically, the reconstruction of the 3D-printed navigation model could delay the time to surgery initiation. Nevertheless, our data showed that time from admission to surgery was 4.7 ± 1.0 h and 4.4 ± 0.9 h for patients in the experimental and control groups, respectively. Nevertheless, the result was not statistically significant, suggesting that 3D-printed navigation technology could not extend the time of preoperative preparation. This is because clinicians need certain preoperative preparation time for activities, such as talking with family members, signing documents, and preparing the operating room. During this period, the reconstruction of the 3D-printed navigation model can be completed. Also, the operation time in the experimental group was significantly

lower than that in the control group (104.3 ± 14.0 min versus 118.6 ± 15.1 min, $P < 0.001$), showing that 3D-printed model-guided endoscopic evacuation shortens the operation and the anesthesia times, thereby reducing the possibility of accidental operation to some extent.

During the operation, the navigation model was placed on the maxillofacial region of the patient. It is important that the fixed puncture hole can reduce the swing of the puncture device during the puncture process and minimize the risk of sudden events and massive bleeding caused by a puncture in the wrong direction. Our results of the number of intraoperative punctures support this advantage, showing that the 3D-printed navigation model increases the convenience and accuracy of endoscopic evacuation, avoiding the possibility of repeated puncture. It could be argued that PHE in the experimental group was smaller than that in the control group on day 7 after the operation (64.3 ± 12.2 mL versus 71.3 ± 13.5 mL, $P = 0.040$). PHE is a radiologic manifestation of secondary brain damage, which is a result of the action of a combination of physical forces in the intracerebral hematoma, the mechanical injury caused by surgery itself, and cytotoxic edema. Previous reports evidenced the clinical significance of PHE, suggesting that PHE affects the functional outcome of ICH patients [29, 30]. Another significant beneficial effect of this novel method is that the evacuation rate of hematoma on postoperative day 1 in the experimental group was significantly higher than that in the control group. Meanwhile, the number of patients treated with urokinase was only two in the experimental group, whereas four cases in the control group were subjected to that treatment. The 3D-printed model-guided endoscopic evacuation in our study also achieved a higher accuracy of puncture. Additionally, statistical analyses revealed no significant association between the two groups in terms of postoperative complications, including rebleeding, infectious meningitis, pulmonary infection, digestive tract ulcer, and epilepsy. Besides, no patient in both groups underwent cerebral infarction and reoperation. Finally, we assessed the outcomes at discharge and the long-term prognosis. Our results showed no significant difference in GCS at discharge, total expenses, in-ICU stay, and in-hospital stay between the two groups. At the 6-month follow-up examination, no statistically significant difference was observed in the mortality rates and GOS score between the two groups. This result confirms that 3D-printed model-guided endoscopic evacuation does not improve the functional prognosis of ICH patients. Based on these findings, further, larger, prospective trials should be undertaken to confirm the effects of 3D-printed model-guided endoscopic evacuation.

Conclusion

In summary, this study confirmed that 3D-printed model-guided endoscopic evacuation has the advantages of minimal operative trauma, shorter operation time, less intraoperative blood loss, and higher hematoma clearance over neuroendoscopic surgery guided by hand-painted localization on the patient's body surface according to the CT marks. In addition, the 3D printing equipment of is inexpensive, and the 3D print-assisted technique is simple to operate with minimal technical difficulty. Therefore, 3D-printed model-guided endoscopic evacuation is not only more rapid and reliable but also has great application prospects and is worthy of promotion in clinical practice.

Acknowledgements We thank Professor Li who helped us with language editing.

Funding This work was financially supported by the Dongguan Social Science and Technology Development (General) Project (No. 2018507150401452).

Declarations

Ethics Approval and Consent to Participate The present study was approved by the Ethics Committee of Tangdu Hospital, Air Force Medical University and Dalang Hospital, Dongguan City, China. All patients in the present study provided written informed consent.

Consent for Publication Study participants provided their consent for the publication of any data/associated images.

Competing Interests The authors declare no competing interests.

References

1. Poungvarin N, Suwanwela NC, Venketasubramanian N, et al. Grave prognosis on spontaneous intracerebral haemorrhage: GP on STAGE score [J]. J Med Assoc Thail. 2006;89(Suppl 5):S84–93.
2. Sacco S, Marini C, Toni D, Olivieri L, Carolei A. Incidence and 10-year survival of intracerebral hemorrhage in a population-based registry [J]. Stroke. 2009;40(2):394–9.
3. Qureshi AI, Mendelow AD, Hanley DF. Intracerebral haemorrhage [J]. Lancet. 2009;373(9675):1632–44.
4. Morgenstern LB, Hemphill JR, Anderson C, et al. Guidelines for the management of spontaneous intracerebral hemorrhage: a guideline for healthcare professionals from the American Heart Association/American Stroke Association [J]. Stroke. 2010;41(9):2108–29.
5. Siddique MS, Fernandes HM, Arene NU, Wooldridge TD, Fenwick JD, Mendelow AD. Changes in cerebral blood flow as measured by HMPAO SPECT in patients following spontaneous intracerebral haemorrhage [J]. Acta Neurochir Suppl. 2000;76:517–20.
6. Mendelow AD, Gregson BA, Rowan EN, Murray GD, Gholkar A, Mitchell PM, et al. Early surgery versus initial conservative treatment in patients with spontaneous supratentorial lobar intracerebral haematomas (STICH II): a randomised trial [J]. Lancet. 2013;382(9890):397–408.
7. Xi G, Keep RF, Hoff JT. Mechanisms of brain injury after intracerebral haemorrhage [J]. Lancet Neurol. 2006;5(1):53–63.

8. Zheng W, Zhang C, Hou D, Cao C. Comparison on different strategies for treatments of hypertensive hemorrhage in the basal ganglia region with a volume of 25 to 35 ml [J]. Acta Cir Bras. 2012;27(10):727–31.
9. Yokosuka K, Uno M. Endoscopic hematoma evacuation for intracerebral hemorrhage[J]. No Shinkei Geka. 2015;43(6):493–506.
10. Takeuchi S, Takasato Y, Masaoka H, Hayakawa T, Yatsushige H, Shigeta K, et al. Decompressive craniectomy with hematoma evacuation for large hemispheric hypertensive intracerebral hemorrhage [J]. Acta Neurochir Suppl. 2013;118:277–9.
11. Xu X, Chen X, Li F, Zheng X, Wang Q, Sun G, et al. Effectiveness of endoscopic surgery for supratentorial hypertensive intracerebral hemorrhage: a comparison with craniotomy [J]. J Neurosurg. 2018;128(2):553–9.
12. Rehman WA, Anwar MS. Surgical outcome of spontaneous supra tentorial intracerebral hemorrhage [J]. Pak J Med Sci. 2017;33(4):804–7.
13. Hoerner MR, Maynard MR, Rajon DA, Bova FJ, Hintenlang DE. Three-dimensional printing for construction of tissue-equivalent anthropomorphic phantoms and determination of conceptus dose [J]. AJR Am J Roentgenol. 2018;211(6):1283–90.
14. Bale SS, Vernetti L, Senutovitch N, Jindal R, Hegde M, Gough A, et al. In vitro platforms for evaluating liver toxicity [J]. Exp Biol Med (Maywood). 2014;239(9):1180–91.
15. Li J, Chen M, Fan X, Zhou H. Recent advances in bioprinting techniques: approaches, applications and future prospects [J]. J Transl Med. 2016;14:271.
16. Keep RF, Hua Y, Xi G. Intracerebral haemorrhage: mechanisms of injury and therapeutic targets [J]. Lancet Neurol. 2012;11(8):720–31.
17. Thabet AM, Kottapally M, Hemphill JR. Management of intracerebral hemorrhage [J]. Handb Clin Neurol. 2017;140:177–94.
18. Mendelow AD. Mechanisms of ischemic brain damage with intracerebral hemorrhage [J]. Stroke. 1993;24(12 Suppl):I115–7 I118-I119.
19. Juttler E, Steiner T. Treatment and prevention of spontaneous intracerebral hemorrhage: comparison of EUSI and AHA/ASA recommendations [J]. Expert Rev Neurother. 2007;7(10):1401–16.
20. Zhang J, Lu S, Wang S, et al. Comparison and analysis of the efficacy and safety of minimally invasive surgery and craniotomy in the treatment of hypertensive intracerebral hemorrhage [J]. Pak J Med Sci. 2018;34(3):578–82.
21. Zhao YN, Chen XL. Endoscopic treatment of hypertensive intracerebral hemorrhage: a technical review [J]. Chronic Dis Transl Med. 2016;2(3):140–6.
22. Mendelow AD. Surgical craniotomy for intracerebral haemorrhage [J]. Front Neurol Neurosci. 2015;37:148–54.
23. Feng Y, He J, Liu B, et al. Endoscope-assisted keyhole technique for hypertensive cerebral hemorrhage in elderly patients: a randomized controlled study in 184 patients [J]. Turk Neurosurg. 2016;26(1):84–9.
24. Di Ieva A, Tam M, Tschabitscher M, et al. A journey into the technical evolution of neuroendoscopy [J]. World Neurosurg. 2014;82(6):e777–89.
25. Li Y, Yang R, Li Z, Yang Y, Tian B, Zhang X, et al. Surgical evacuation of spontaneous supratentorial lobar intracerebral hemorrhage: comparison of safety and efficacy of stereotactic aspiration, endoscopic surgery, and craniotomy [J]. World Neurosurg. 2017;105:332–40.
26. Malik HH, Darwood AR, Shaunak S, et al. Three-dimensional printing in surgery: a review of current surgical applications [J]. J Surg Res. 2015;199(2):512–22.
27. Fu C, Wang N, Chen H, Chen Q. A novel simple puncture positioning and guidance system for intracerebral hematoma [J]. World Neurosurg. 2019;131:e562–9.
28. Wang Q, Guo W, Liu Y, Shao W, Li M, Li Z, et al. Application of a 3D-printed navigation mold in puncture drainage for brainstem hemorrhage [J]. J Surg Res. 2020;245:99–106.
29. Venkatasubramanian C, Mlynash M, Finley-Caulfield A, Eyngorn I, Kalimuthu R, Snider RW, et al. Natural history of perihematomal edema after intracerebral hemorrhage measured by serial magnetic resonance imaging [J]. Stroke. 2011;42(1):73–80.
30. Yang J, Arima H, Wu G, Heeley E, Delcourt C, Zhou J, et al. Prognostic significance of perihematomal edema in acute intracerebral hemorrhage: pooled analysis from the intensive blood pressure reduction in acute cerebral hemorrhage trial studies [J]. Stroke. 2015;46(4):1009–13.